Available online at www.sciencedirect.com
SCIENCE DIRECT®
Geochimica et Cosmochimica Acta 70 (2006) 2919–2934
Geochimica
www.elsevier.com/locate/gca

Light lithophile elements in pyroxenes of Northwest Africa (NWA) 817 and other Martian meteorites: Implications for water in Martian magmas

Allan H. Treiman [a,*], Donald S. Musselwhite [a], Christopher D.K. Herd [b], Charles K. Shearer Jr. [c]

[a] *Lunar and Planetary Institute, 3600 Bay Area Boulevard, Houston, TX 77058, USA*
[b] *Department of Earth and Atmospheric Sciences, I-26 Earth Sciences Bldg, University of Alberta, Edmonton, Alta., Canada T6G2E3*
[c] *Institute of Meteoritics, University of New Mexico, Albuquerque, NM 87754, USA*

Received 15 August 2005; accepted in revised form 10 March 2006

Abstract

Zoning patterns of light lithophile elements (the LLE: Li, Be, and B) in pyroxenes of some Martian basaltic meteorites have been used to suggest that the parent basalts were saturated in water and exsolved an aqueous fluid phase. Here, we examine LLE zoning in the augites of a quickly cooled Martian basalt that was not water-saturated—the Northwest Africa (NWA) 817 nakhlite. Analyses for LLE were by secondary ion mass spectrometry (SIMS), supported by EMP analyses of major and minor elements. In NWA 817, zoning of Be and B is consistent with igneous fractionations while Li abundances are effectively constant across wide ranges in abundance of other incompatible elements (Be, B, Ti, and Fe*). The lack of strong zoning in Li can be ascribed to intracrystalline diffusion, despite the rapid cooling of NWA 817. Most other nakhlites, notably Nakhla and Lafayette, cooled more slowly than did NWA 817 [Treiman, A.H., 2005. The nakhlite Martian meteorites: augite-rich igneous rock from Mars. *Chem. Erde* **65**, 203–270]. In them Li abundances are constant across augite, as are abundances of other elements. In Nakhla pyroxenes, all the LLE have effectively constant abundances across significant ranges in Fe* and Ti abundance. Lafayette is more equilibrated still, and shows constant abundances of LLE and nearly constant Fe*. A pyroxene in the NWA480 shergottite has constant Li abundances, and was interpreted to represent mineral fractionation coupled with exsolution of aqueous fluid. A simple quantitative model of this process requires that the partitioning of Li between basalt and aqueous fluid, $^{Li}D_{aq/bas}$, be 15 times larger than its experimentally determined value. Thus, its seems unlikely that the Li zoning pattern in NWA480 augite represents exsolution of aqueous fluid. Late igneous or sub-solidus diffusion seems more likely as is suggested by Li isotopic studies [Beck, P., Chaussidon, M., Barrat, J.-A., Gillet, Ph., Bohn, M., 2005. An ion-microprobe study of lithium isotopes behavior in nakhlites. *Meteorit. Planet. Sci.* **40**, Abstract #5118; Beck, P., Chaussidon, M., Barrat, J.-A., Gillet, Ph., Bohn, M., 2006. Diffusion induced Li isotopic fractionation during the cooling of magmatic rocks: the case of pyroxene phenocrysts from nakhlite meteorites. *Geochim. Cosmochim. Acta* **70**, in press]. Pyroxenes of the Shergotty and Zagami meteorites have nearly constant abundances of B, and Li that decreases core-to-rim. Applying the quantitative model to the constant B in these pyroxenes requires that $^{B}D_{aq/bas}$ be 25 times larger than experimentally constrained values. Li abundances in pigeonite can be fit by the model of crystal fractionation and fluid loss, but only if $^{Li}D_{aq/bas}$ is 30 times the experimentally constrained value. The Li abundance pattern in augite cannot be modeled by simple fractionation, suggesting some strong crystal-composition effects. Thus, Li and B distributions in Shergotty and Zagami pyroxenes cannot be explained by igneous fractionation and exsolution of aqueous vapor. Intracrystalline diffusion, complete for B and incomplete for Li, seems more consistent with the observed zoning patterns.

1. Introduction

Water is a major focus of Mars exploration, and recent spacecraft missions provide strong evidence that water ice

* Corresponding author.
E-mail address: treiman@lpi.usra.edu (A.H. Treiman).

0016-7037/$ - see front matter © 2006 Elsevier Inc. All rights reserved.
doi:10.1016/j.gca.2006.03.008

is now abundant in Mars' regolith (Boynton et al., 2002), and that liquid water was once a potent geologic agent (e.g., Carr and Head, 2003). However, the source of the surface water is not clear—some of the water was derived from external (meteoritic) sources (Karlsson et al., 1992), and some was likely derived from volcanic outgassing (Greeley, 1987). The abundance of water from volcanic outgassing is uncertain, because the Martian meteorites (all basaltic rocks) show nearly no signs of having contained magmatic water. They now contain less than 100–200 ppm H_2O that could have been magmatic (Leshin et al., 1996). The meteorites contain potentially water-bearing minerals like apatite and amphibole, but these are nearly devoid of water (Watson et al., 1994). Liquidus equilibria of the Martian meteorites could indicate whether their parent magmas were dry or water rich, but melting equilibrium experiments on shergottite compositions are consistent with both states (Stolper and McSween, 1979; Dann et al., 2001). On the other hand, water-rich basaltic magma could produce dry basaltic rock, and McSween et al. (2001) and Lentz et al. (2001) hypothesized that water was lost from the shergottite magmas to aqueous fluid during crystallization.

To test their hypothesis of water loss, McSween et al. (2001) and Lentz et al. (2001) analyzed abundances of light lithophile elements, the LLE (Li, Be, and B), in pyroxenes in the Martian basaltic meteorites Shergotty, Zagami, Nakhla, and Lafayette. Lithium and boron are good probes of water loss, because they are incompatible in silicate minerals compared to basalt magma (e.g., Brenan et al., 1998a; Herd et al., 2004) but are soluble in high-temperature aqueous fluids, Table 1 (Brenan et al., 1998b). Thus, abundances of Li and B in basaltic magma should increase as it crystallizes, and decrease as aqueous fluid (liquid or supercritical) is exsolved and lost. Pyroxene grains growing in the magma should record these changes in Li and B (e.g., Papike, 1996). In pyroxenes of the Martian basalts Shergotty and Zagami, McSween and Lentz found that abundances of Li and B decrease from core to rim, i.e., over time and crystallization. Thus, McSween and Lentz inferred that partitioning among basalt and silicate minerals could not produce the core-to-rim decreases in Li and B, and invoked loss of aqueous fluid.

This argument for water-loss assumes implicitly that Li and B followed instantaneous chemical equilibria among basalt magma, silicate minerals, and aqueous fluid (McSween et al., 2001; Lentz et al., 2001). We have tested the equilibrium behavior of Li and B between minerals and magma (Herd et al., 2004, 2005), and now extend that study to a natural Martian example.

The North West Africa (NWA) 817 nakhlite is particularly appropriate for investigating the igneous behavior of the LLE. It is among the most rapidly cooled of the Martian meteorites (Sautter et al., 2002; Treiman, 2005) and so should have been affected little by high-temperature redistribution of elements. Also, it experienced minimal shock (Sautter et al., 2002; Treiman, 2005), and so should not be strongly affected by element redistribution from shock-induced heating (Chaklader et al., 2004, 2005). Finally, NWA 817 and the other nakhlites show no indication that their parent magmas contained significant water, nor that they experienced exsolution of an aqueous fluid phase (McSween et al., 2001; Lentz et al., 2001). Thus, NWA 817 provides a "pure play" for extending experimental studies of mineral/basalt equilibria of LLE to Martian conditions.

Table 1
Partition coefficients-D values[a]

	Li	Be	B	Ti
$D_{aug/bas}$	0.2–0.35[b,d,f]	0.015[b]	0.035[b,f]	0.3–0.6[f,k,l,m]
$D_{pig/bas}$	0.2[e,f,j]	0.015[o]	0.02[b,f,i]	0.15[f,k,l,m]
$D_{ol/bas}$	0.25[b,f,j]	0.002[b]	0.007[b,f]	0.0[o]
$D_{pl/bas}$	0.3[b,c,f,j]	0.27[b]	0.024[b,f]	0.0[o]
$D_{mer/bas}$	0.7[f]	—	0.03[f]	0.0[o]
$D_{aq/bas}$	2.5[g]	0.01	0.3–0.5[h] 1.1–2.0[g]	0.0[n]

Abbreviations used: bas, basaltic magma; aug, augite pyroxene; pig, pigeonite pyroxene (includes data of [6] for orthopyroxene); ol, olivine; pl, plagioclase; mer, merrillite; aq, aqueous fluid.

[a] Mass distribution ratio for an element between two phases, i.e., $^{El}D_{ol/bas}$ = [Li in olivine/Li in basalt magma].

[b] Brenan et al. (1998a).

[c] Bindeman et al. (1998).

[d] Gaetani et al. (2003).

[e] McDade et al. (2003).

[f] Herd et al. (2004).

[g] Lentz et al. (2001).

[h] Hervig et al. (2002).

[i] Chaussidon and Libourel (1993).

[j] Ryan (1989).

[k] Johnson (1998).

[l] Dann et al. (2001).

[m] Johnston and Schwab (2004).

[n] Estimated from Ayers and Watson (1993).

[o] Estimated.

We find that the behavior of Be and B in the augites of NWA 817 is consistent with simple igneous fractionation and with experimentally determined partition coefficients. However, Li does not share this simple behavior, and its distributions in augite are more consistent with extensive intra- and inter-crystalline diffusion. From this discovery, we consider whether the zoning patterns of Li, B, and Be in pyroxenes of other Martian meteorites (Nakhla, Lafayette, NWA480, Shergotty, and Zagami) are consistent with igneous fractionation. In fact, none of the chemical zoning patterns of Li and B in these meteorites' pyroxenes is consistent with simple fractionation using established mineral/basalt partition coefficients (Table 1). Chemical zoning patterns for Be are consistent with igneous mineral/basalt fractionation in some of the Martian meteorites, but not in others. It seems likely that the distributions of Li and B in these other Martian meteorites were modified by diffusion (enabled by protracted cooling, shock heating, or other processes).

1.1. NWA 817

The NWA 817 meteorite was recovered from the Sahara desert in 2000. It is a nakhlite, an olivine-bearing

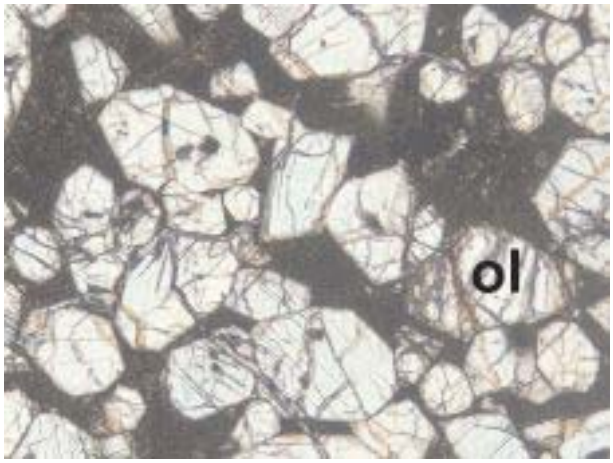

Fig. 1. NWA 817 in thin section. General view, showing euhedral zoned augite (clear) and olivine (ol) crystals in a fine-grained, brown and black groundmass. Plane light, 2.3 mm across image (Treiman, 2005).

clinopyroxenite with elemental and isotopic parameters consistent with the Nakhla meteorite and other similar stones inferred to be from Mars (Sautter et al., 2002; Treiman, 2005). NWA 817 consists of ~69% (volume) of sub-calcic augite pyroxene, ~12.5% olivine, and ~18.5% fine-grained mesostasis material among the augite and olivine. The augite occurs as euhedral or subhedral grains ~1 mm long and ~0.3 mm across (Figs. 1 and 2). They are strongly zoned in chemical composition from large, relatively magnesian cores to thin, highly ferroan rims. The increasing Fe* [molar Fe/(Fe + Mg)] in the rim zones is closely correlated with increases in abundances of incompatible element like Ti, Al, Y, and the REE (Fig. 3; Wadhwa et al., 2004; Treiman, 2005). The outermost rims show distinct decreases in Ca content, tending toward ferrosilitic pigeonite. The olivine grains are euhedral to subhedral and approximately the same size as the pyroxenes (and slightly larger), and commonly enclose small augite grains or extend between them. The olivines, too, show strong chemical zoning, Mg' from 41% to 14% (Sautter et al., 2002; Mikouchi et al., 2003). Among these large olivine and pyroxene grains is fine-grained mesostasis material, consisting of elongate laths of plagioclase feldspar, silicic glass, augite and pigeonite pyroxenes, titanomagnetite in dendritic and cellular crystals, and minor Cl-apatite and pyrrhotite (Sautter et al., 2002; Treiman, 2005). The texture of the mesostasis suggests very rapid cooling (Sautter et al., 2002), as does the strong chemical zoning in the olivine (Mikouchi et al., 2003).

2. Sample and methods

Analyses here are from a thin section of NWA 817, cut by Treiman from a fragment of the meteorite from M. Fectay and C. Bidaut (La Memoire de la Terre). This material is identical in petrography and mineral chemistry (see Treiman, 2005) to the type sample described by Sautter et al. (2002). Our emphasis is on chemical zoning in the large augite grains, which are the only analyses reported here. In general, studies of mineral chemical zoning consider only grains where the zoning is perpendicular to the section surface—only in this orientation can mineral zoning be used for quantitative determination of diffusion rates, overgrowth volumes, etc. However, the rim zones in augites of NWA 817 are relatively narrow compared to the analytical spot size of the SIMS (see below). Thus, we selected grains that showed the widest Fe-enriched rim zones (as judged by BSE imagery; Fig. 2). These grains must have their crystal faces oriented at shallow angles to the plane of the thin section, so that 'planes' of constant chemical composition are also at shallow angles to the thin section plane. In this way, our SIMS analyses are of relatively homogeneous pyroxene. Conversely, the zoning profiles here *cannot* be used for quantitative modeling that depends on scales of length, area, or volume.

Backscattered electron (BSE) images were obtained, and major and minor elements were analyzed, using the Cameca SX-100 electron microprobe (EMP) at the NASA Johnson Space Center (Appendix A). Analyses were all in wavelength-dispersive mode, using an electron beam of 15 kV accelerating potential and a current of 20 nA (Faraday cup). Count times were 30 s on peaks, and the same total for backgrounds. Standards were well-characterized natural amphibole (Kakanui), natural garnet (NVGR), and pure Cr metal. Data were reduced with the Cameca PAP software, which uses a $\varphi - \rho - Z$ algorithm. Nearly all analyses had acceptable analytical sums (99–100.5%wt), and proper pyroxene stoichiometry (for 6 O atoms, one has nearly 2 Si, and less than one Ca, Appendix A). These analyses are consistent with others of NWA 817 augites taken with the same instrument at other times (Treiman, 2005) and with other instruments (Sautter et al., 2002). While stoichiometry is satisfied, the total cation charge is slightly less than needed to balance the anion (oxygen) charge in the augite formulae. This imbalance is consistent with ~10% of the iron in the augite being ferric (see Dyar et al., 2005). Unless otherwise stated, percentages of oxides given are weight percent (%wt).

Spots in augite grains were analyzed for the LLE using the Cameca IMS 4f ion microprobe at the University of New Mexico, Department of Earth and Planetary Sciences and Institute of Meteoritics (Appendix A). Analysis included ^{7}Li, ^{9}Be, ^{11}B, ^{30}Si, ^{42}Ca, and ^{48}Ti. Analyses were made by bombarding the sample with primary O^- ions at a nominal potential of 10 kV. A primary ion current of 10 nA was focused on the sample to a spot diameter of 10–15 μm. Sputtered secondary ions were energy filtered using a sample offset voltage of 75 V, and an energy window of ±25 eV, to eliminate isobaric interferences. ^{42}Ca and ^{48}Ti were used principally as aids in navigating the sample. We used peak counting times of 5 s on ^{7}Li and ^{11}B, and 10 s on ^{9}Be. Absolute concentrations of each element were calculated using empirical relationships of measured peak/^{30}Si ratios normalized to known SiO_2 content from EMP analyses of the same spots. LLE standards include Plagioclase C, Webster-Addie augite (WAA), glasses NBS610 and NBS612; San Carlos

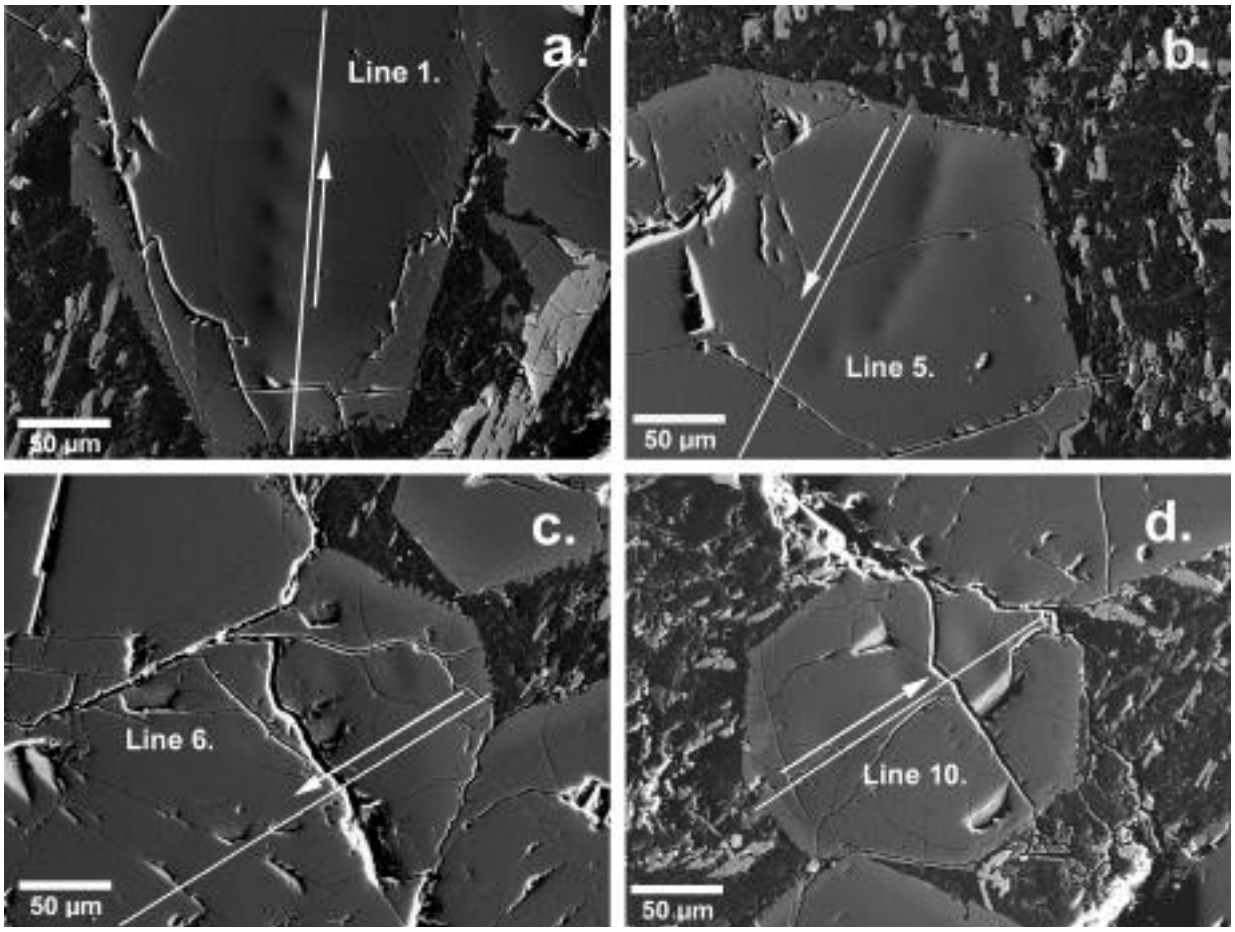

Fig. 2. Analyzed augite grains, mixed SEI/BSE images taken after SIMS analyses. Straight white lines are loci of EMP analyses, arrows show increasing distance as in Fig. 3 and Appendix. SIMS analytical spots are pits near those lines. (a) Augite grain with Line 1. (b) Augite grain with Line 5. Analytical traverse starts at grain rim. (c) Augite grain with Line 6. Analytical traverse starts at grain rim. (d) Augite grain with Line 10. Analytical traverse starts at grain rim to lower left.

olivine (SK59) was used also for Li and B only (Herd et al., 2004, 2005). To minimize contamination by B adsorbed on the sample surface, thin sections were soaked for 2 h in 1% mannitol solution following the procedure of Lentz et al. (2001), and rinsed in ultrapure (18 MΩ) water. Samples were carbon-coated immediately after mannitol treatment and cleaning. In addition, the ion beam was rastered over the sample for 4 min, and then placed in point mode and allowed to bore for another 2 min before acquiring each analysis, following the procedure outlined by Herd et al. (2004). In a few cases, ion counts for B decreased over time, indicating residual contamination; in these cases, we used only the later replicate analyses after count rates had stabilized. Ion imaging was utilized to select spots for analysis; because fractures are traps for alumina polishing powder, they could be avoided by imaging Al ions. Data are presented in the Appendix A with 1σ uncertainties from counting statistics and standardization. All analyses for Li and most analyses for B are statistically significant, i.e., the analyzed value is several times (or more) its 2σ uncertainty. Analyses for Be are statistically significant only at the higher concentrations of the augite rims (Appendix A). Analyses for Be in the augite cores are at or below detection limits.

2.1. Igneous behavior of LLE

The equilibrium distributions of trace elements like Li, B, and Be among phases are conventionally given as partition coefficients, D values, the mass ratios of the trace element abundances in two phases. For instance, the standard notation for the partition coefficient for lithium between olivine and basaltic magma is ${}^{\mathrm{Li}}D_{\mathrm{ol/bas}} = [\mathrm{Li\ in\ olivine}/\mathrm{Li\ in\ basalt\ magma}]$. Values used here, and their sources, are given in Table 1 with the abbreviations: pig, pigeonite pyroxene; px, pyroxenes in general; pl, plagioclase; ol, olivine; and mer, merrillite. The most critical data here are for distribution between aqueous fluid and basalt magma, $D_{\mathrm{aq/bas}}$, and they are unfortunately the poorest known. There are a few direct determinations for B (Hervig et al., 2002), but values for Li and Be are extrapolated from $D_{\mathrm{aq/aug}}$ and $D_{\mathrm{aug/bas}}$ (Lentz et al., 2001), which are typically for different temperatures and augite compositions. So, these values must be taken as indicative rather than exact. If anything, actual $D_{\mathrm{aq/bas}}$ will likely be closer to unity than the estimated values, because the compositions of the aqueous fluid and the basaltic melt will converge as temperature increases (by analogy with the results of Jones et al., 1995).

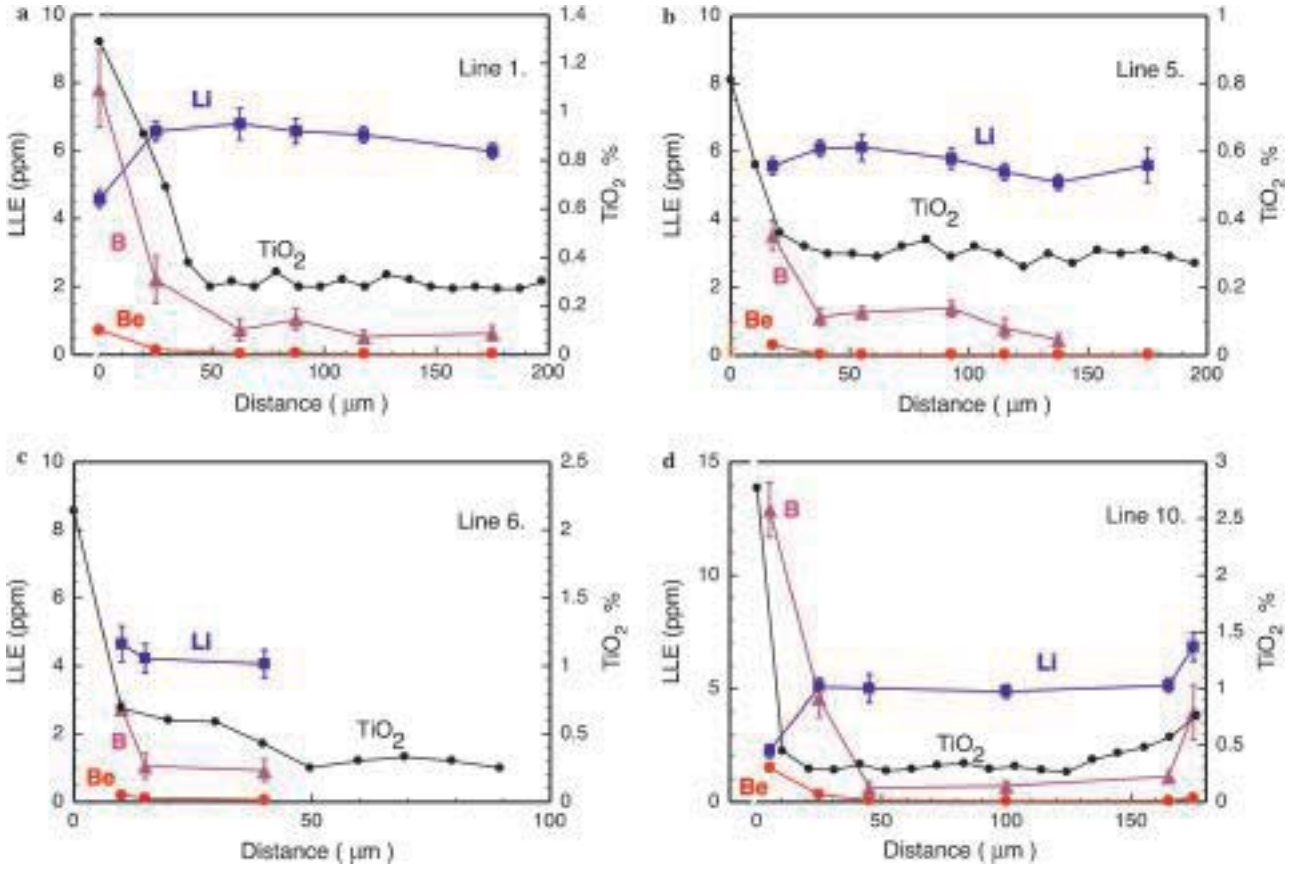

Fig. 3. Element abundances and ratios in traverses across augites in NWA 817 (Appendix). Abundances of Ti are by EMP on the lines of Fig. 2; Li, Be, and B abundances by SIMS, uncertainty bars 1σ. (a) Line 1, Fig. 2a. Traverse from sharp zoned rim into core. Li abundances essentially constant inside grain, and lower at its rim. (b) Line 5, Fig. 2b. Traverse from sharp zoned rim into core. (c) Line 6, Fig. 2c. Plateau rim from 10 to 30 μm into core (>50 μm). (d) Line 10, Fig. 2d. Sharp rim to the left shows 10-fold enrichments in Ti and B from core to grain edge, accompanying a change in Fe* from 0.38 to 0.90, while Li abundances *decrease* by a factor of two. The plateau rim on the right of the figure (~140–160 μm), shows only modest increases in Ti, Li, B, and Fe*.

We use titanium abundances in pyroxene as a proxy for the extent of igneous fractionation, as is commonly done with Martian basaltic rocks (e.g., Harvey et al., 1993; Lentz et al., 2001; Beck et al., 2004; Herd et al., 2004, 2005; Day et al., 2006). This use of Ti is appropriate in considering magmas that might exsolve an aqueous phase, as Ti is minimally soluble in it. To first order, mineral/basalt distribution coefficients for Ti are known (Table 1), although substitution of Ti into pyroxenes must be coupled by charge-balance to other substitutions, like $^{VI}Mg^{2+} + 2\,^{IV}Si^{2+}IV = {}^{VI}Ti^{2+} + 2\,{}^{IV}Al^{2+}$ (Papike et al., 2005). These coupled substitutions tie Ti abundances to those of other minor elements in pyroxene, and make it less than ideal as a proxy for the extent of igneous fractionation. In our opinion and those of the above references, Ti remains the best available elemental proxy, measurable by electron microprobe, for extent of fractionation. Raw Al abundances in pyroxene change dramatically when plagioclase begins to crystallize, while Ti abundances do not. Abundances of Na and Cr are commonly too imprecise, and the Fe/Mg ratio is readily disturbed by diffusion (e.g., Harvey et al., 1993; Treiman, 2005).

3. Results: NWA 817 augite

NWA 817 is among the most rapidly cooled of the Martian meteorites (along with Y980459 and MIL03346), and so is likely to retain pristine igneous characteristics (Sautter et al., 2002; Mikouchi et al., 2003; Treiman, 2005). We obtained chemical analyses of augites in NWA 817 using EMP for major and minor elements, and using SIMS for Li, Be, and B (Figs. 2 and 3; see Appendix A for analyses). Musselwhite et al. (2005) gave a preliminary report of some of these data. As noted above, the analytical traverses are on grains oriented so that the Fe-enriched rim zones appear as wide as possible. This permits SIMS spots to occupy areas of relatively constant compositions, but makes these traverses unsuitable for applications that require knowing lengths (i.e., volumes of crystallization or length scales of diffusion). Correlation of the locations of EMP and SIMS analytical spots was based on BSE and SEI images of the pyroxenes before and after analyses, and is necessarily imprecise as the SIMS analytical volume is broader than that of EMP.

3.1. Core zones

Data for our analytical traverses of NWA 817 augites are presented in Fig. 3 and tabulated in the Appendix A. As in the other nakhlites, augite grains in NWA 817 have core regions of relatively constant Fe* and relatively constant abundances of incompatible elements like Ti and Al (Fig. 3; Sautter et al., 2002; Wadhwa et al., 2004; Treiman, 2005). Spots in the cores show high concentrations of Al and other incompatible elements (including Be and B; Fig. 2a, profile 1), which are probably associated with magmatic inclusions (Varela et al., 2001; Stockstill et al., 2005). Core compositions vary somewhat from grain to grain in a single nakhlite (Treiman, 2005); for instance, TiO_2 in core augite from NWA 817 ranges from 0.24–0.32% (Appendix A, Figs. 3 and 6; Sautter et al., 2002). This could be an artifact of thin sectioning—higher TiO2 values might be recorded where the thin section plane was offset from the augite grain's true center. The LLEs show similar, though greater, ranges of core augite compositions: Li from 4 to 6 ppm, B from 0.6 to 2 ppm, and Be from 20 to 60 ppb (Figs. 3 and 6). Beck et al. (2005, 2006) report larger core Li abundances, averaging 9 ppm, and also find that the Li isotopic composition is not constant—δ^7Li ranges from −12‰ to +22‰.

3.2. Rim zones

Surrounding the augite cores are rim zones marked by increasing Fe* and increasing abundances of incompatible elements like Ti, Al, Y, and the REE (Figs. 2 and 3; Sautter et al., 2002; Wadhwa et al., 2004; Treiman, 2005). We found two distinct types of rim zoning: sharp and plateau.

Sharp rims show a strong monotonic increase in Fe* and Ti from the core outwards (Fig. 3). In sharp rims, TiO_2 increases from a typical core value of ~0.25% to a maximum near 2%. This normal, single-stage igneous zoning is common in most nakhlites: NWA 817 (Sautter et al., 2002), Nakhla (Treiman, 1990; Harvey and McSween, 1992; Friedman-Lentz et al., 1999), Governador Valadares (Friedman-Lentz et al., 1999), Y000593 and its pairs (Imae et al., 2003), and MIL03346 (McKay and Schwandt, 2005; Treiman, 2005).

Several augite rims in NWA 817 show a different pattern, in which monotonic increases in Fe* and Ti abundance are interrupted by plateaus of constant composition, or even slight decreases in Fe* and Ti, etc. In plateau rims analyzed here, chemical zoning is not as strong as in the sharp rims. In plateau rims, TiO_2 increases to only ~0.6%, compared to the sharp rim value of ~2%. The distribution of sharp and plateau-type rims seems random, and the grain of profile 10 has a sharp rim on one side and a plateau rim on the other (Fig. 3). The plateau rims are found adjacent to mesostasis material (Figs. 2c,d and 3c,d), and so do not represent grain edges that are blocked from access to mesostasis magma (e.g., Fig. 4a of Imae et al., 2003).

For the most part, abundances of Be and B follow those of Ti and other incompatible elements in the NWA 817 augites—they increase rapidly in sharp zones (profile 6 and left side of profile 10; Fig. 3), and show plateaus in plateau rims (profiles 10R and 5, Fig. 3). Abundances of Be and B increase to greater proportions than do those of Ti; e.g., profile 10L shows a 10-fold increase in Ti and 20-fold increases in B and Be (Fig. 3). This parallel behavior, but more extreme for B and Be, is consistent with normal igneous partitioning of incompatible elements—Ti having larger $D_{aug/bas}$ than B and Be (Table 1). This relation is quantified in Fig. 4, which shows element abundances in rim zones normalized to their average abundances in the adjacent augite cores.

Fig. 4 shows that Be and B become more strongly enriched in the augite rims than does Ti—the considerable scatter in the plotted points can be ascribed to analytical uncertainties in Be and B, and imprecise registry of Ti values (from EMP) with Be and B values (from SIMS)—see Fig. 2. The enrichment trends of Fig. 4 can be modeled by simple Rayleigh fractional crystallization. Boron and beryllium are nearly completely incompatible into pyroxene: $^{B}D_{aug/bas} \sim 0.035$ and $^{Be}D_{aug/bas} \sim 0.015$ (Table 1: Lentz et al., 2001; Herd et al., 2004), and Ti is significantly more compatible. The data of Fig. 4 can be matched (with much scatter) using these D values for Be and B, and $^{Ti}D_{aug/bas} \sim 0.5$. This value for $^{Ti}D_{aug/bas}$ is larger than measured from experiments on shergottite Martian basalts (Herd et al., 2004), but is consistent with other natural systems (e.g., Johnston and Schwab, 2004). Thus, it seems clear that B and Be in the NWA 817 augites retain their magmatic abundances and zoning.

Lithium behaves quite differently. In some analytical traverses, Li increases as the rim is approached (Figs. 3c and d, right side), but never as strongly as anhydrous igneous partitioning would suggest (Fig. 4 and Table 1). In other traverses, Li abundances are effectively constant from core through rim (Fig. 3b; Beck et al., 2005, 2006), which would be consistent with anhydrous igneous partitioning

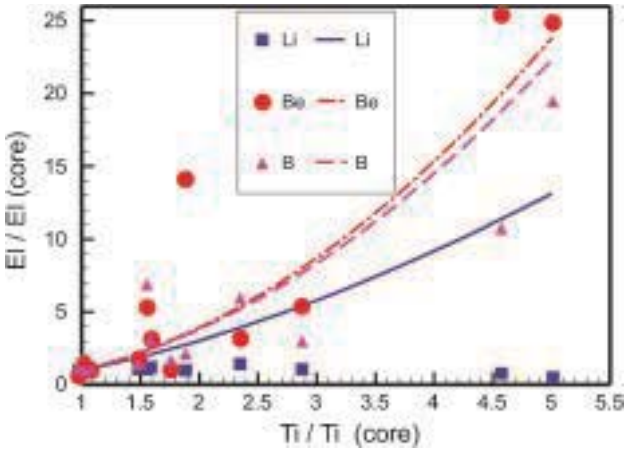

Fig. 4. Fractionation of LLE in NWA 817 augites. Graph shows element abundance enrichments relative to the core augite compositions, as compared to ideal fractionation paths using $^{Ti}D_{aug/bas} = 0.5$ (Table 1). Ti values from EMP, LLE values from SIMS. Much of the scatter can be attributed to analytical uncertainties in LLE, and to misregistry of Ti and LLE analyses.

only if $^{Li}D_{aug/bas} = 1$, which it is not (Table 1). If another phase were fractionating along with augite, it would have to have $^{Li}D_{phase/bas} \gg 1$, because augite was the dominant-crystallizing mineral in NWA 817. Olivine co-crystallized with augite (Sautter et al., 2002; Treiman, 2005), but it supports only $^{Li}D_{ol/bas} = 0.15$–0.35 (Table 1). Fractionation of Li into a fugitive volatile phase is not likely as the nakhlite parent magmas are inferred to have been dry (Lentz et al., 2001).

Lithium abundances even decrease from core to rim in other NWA 817 augites, as in Fig. 3a and the left side of Fig. 3d. The cause of these Li decreases is not known. It cannot be an igneous signature, for the nakhlites contain no phase that would partition Li so strongly away from augite (see Herd et al., 2004). If the constancy of Li abundances in other grains is ascribed to high-temperature diffusion (below), these depletions must post-date the diffusive episodes. The Li depletions could be related to the aqueous alteration experienced by all nakhlites, that converted some of their olivine and mesostasis glasses to smectite clays (Treiman et al., 1993; Gillet et al., 2002; Treiman, 2005).

3.3. Summary on NWA 817

In augites of NWA 817, the LLE display contrasting zoning patterns and hence geochemical behaviors. The zoning patterns of Be and B in the augites are consistent with igneous fractionation (Figs. 3 and 4) as modeled with the augite/basalt partition coefficients of Table 1. On the other hand, the zoning patterns of Li are difficult to explain by igneous fractionation using known partition coefficients (Figs. 3 and 4; Table 1).

The constancy of Li across many augites in NWA 817 cannot result from igneous processing unless the bulk Li partition coefficient for the crystallizing assemblage was unity. Augite and olivine are the only minerals that crystallized early in NWA 817, and they both have ^{Li}D values well below unity (Table 1). Thus, an igneous origin for the constancy of Li abundances is not credible.

An obvious alternative explanation is that Li has diffused rapidly through the NWA 817 augites, so that all original zoning has been erased or strongly subdued. The limited available data on diffusion of Li in silicates suggest that it diffuses much more readily than do other cations. We find no literature data on Li diffusion in pyroxene, and so rely on analogies to diffusion in silicate melts, especially the comprehensive study of Richter et al. (2003). They found that Li diffuses in silicate melts as rapidly as does hydrogen, with a diffusion constant two orders of magnitude larger than those of divalent cations (Ca, Fe, Mg), and $2\frac{1}{2}$ orders of magnitude larger than higher-valency cations (B, Ti). From these data, it seems reasonable to expect that Li will diffuse much more rapidly in pyroxenes than do divalent and higher-valent cations. Thus, one could reasonably expect to encounter pyroxenes in which Li abundances were equilibrated through diffusion, but in which abundances of other elements showed small or undetectable effects of diffusion.

The Li isotope and abundance measurements of Beck et al. (2005, 2006) provide a compelling case for diffusional exchange of Li. They analyzed Li abundances and isotope ratio across two augite crystals in NWA 817, and found that the overall abundance of Li (principally ^{6}Li) was constant while the isotopic composition varied from $\delta^7Li = 0‰$ in the core to $+22‰$ at the rim. This variation in δ^7Li can be explained if the two Li isotopes diffuse through augite at significantly different rates, and the difference is consistent with kinetic models of atomic mobility.

The strong decreases in Li at the rims of some augites are clearly not related to igneous processing, because no minerals in NWA 817 would sequester Li much more than would augite (Table 1). The cause of the rim Li decreases is not known, but could involve loss of Li to a late-crystallizing minor mineral with a very high $^{Li}D_{min/melt}$, or to an aqueous fluid. If a fluid were involved, it would be tempting to correlate it with the fluid that produced the low-temperature smectite-rich alterations in NWA 817 (Newsom et al., 2001; Gillet et al., 2002).

4. LLE in other nakhlites

Armed with these data and inferences from NWA 817, one can interpret the LLE zoning in other nakhlites. The nakhlites all have nearly identical bulk compositions, and core compositions for their augite grains (Treiman, 2005), suggesting that they arose from the same or substantially similar magmas. Most of the differences among nakhlites can be ascribed to post-igneous cooling or later metamorphic equilibration: the MIL 03346 nakhlite cooled fastest, followed by NWA 817. Nakhla itself had an intermediate cooling rate, while Lafayette and NWA998 cooled slowest (Treiman, 2005).

In MIL03346, the augite crystals are strongly zoned in both Li abundances and isotopic ratio (Beck et al., 2005, 2006). Abundances of Li increase from core to rim, but the Li isotopic composition varies in the intermediate zones of the augite. Beck et al. (2005, 2006) interpret this pattern as reflecting partial exchange of Li in the augite with that in the mesostasis, with the Li isotopic variation arising from the different mobilities of the two Li isotopes. Thus, even in the most rapidly cooled nakhlite, there is evidence that Li in augites do not retain a purely igneous distribution pattern.

The Nakhla nakhlite cooled at an intermediate rate (Treiman, 2005), and its augite grains retain igneous zoning patterns; Fe* increases from core to rim, and abundances of Ti and most trace elements increase 2-fold from lowest to highest (Lentz et al., 2001). Lentz et al. (2001) report that its augites have constant abundances of all LLE from core to rim, but Beck et al. (2005) report that rim Li abundances are twice that of the cores. Thus, data for Nakhla appear contradictory—some of its augites may retain igneous zoning of Li (and other LLE?) and others do not.

The Lafayette nakhlite cooled much slower that others considered here, as shown by its textures and the relative homogeneity of its augite compositions (Treiman, 2005).

Most augite grains have little zoning in Fe*, and some have constant Fe*. Many Lafayette pyroxenes retain significant zoning in their Ti contents, which reflects the slower intracrystalline diffusion of Ti compared to Mg or Fe. The Lafayette augite grains have constant abundances of the LLE, independent of their Fe* or Ti content (Lentz et al., 2001).

To summarize, only for Nakhla is there evidence that augite retains igneous zoning patterns for Li. Even in MIL03346, the most rapidly cooled, Li isotope ratios bespeak diffusional exchange with its mesostasis (Beck et al., 2005). Beryllium and boron have been analyzed (besides this work) only for Nakhla and Lafayette (Lentz et al., 2001); across those meteorites' augite grains, abundances of Be and B are constant, even though abundances of Ti and other trace elements are strongly zoned. For MIL 03346, post-igneous intercrystalline and intracrystalline diffusion is indicated (Beck et al., 2005), and one can reasonably infer that the other, more slowly cooled nakhlites, experienced similar or more extensive post-igneous diffusion.

5. LLE in shergottites: aqueous fluids?

The shergottites are basaltic igneous rocks, inferred to be from Mars, containing nearly equal proportions of pigeonite, augite, and plagioclase (shock-transformed to glass). Plagioclase crystallized after pigeonite and augite. The water content of the shergottites' parent magmas is not known with certainty. The magmas may have been hydrous or water-saturated (McSween and Harvey, 1993; McSween et al., 2001; Dann et al., 2001; Lentz et al., 2001), even though the meteorites contain only traces of minerals (kaersutite and apatite) that might have contained hydroxyl or water. Conversely, there is equally good evidence that the magmas contained little water (Stolper and McSween, 1979; Jones, 2004). This apparent contradiction, wet parent magmas and dry basaltic rocks, was explained by the near-complete loss of water from the magma while it was crystallizing (McSween et al., 2001; Lentz et al., 2001; Beck et al., 2004). Lithium and boron, being relatively soluble in aqueous fluid compared to basalt magma (Table 1) would be lost from the basalt into the fluid, and augite phenocrysts would record this loss as decreasing abundances of Li and B from core to rim (Lentz et al., 2001). This scenario can be evaluated quantitatively in a simple model of LLE fractionation during pyroxene crystallization and exsolution of aqueous fluid from basalt magma. Anticipating our conclusions, this water-loss model would seem to require that $^{Li}D_{aq/bas}$ and $^{B}D_{aq/bas}$ be far larger than current estimates or determinations of their values.

5.1. Li in NWA480: a quantitative model

The shergottite NWA480 is similar to Zagami in its petrography and chemistry (Barrat et al., 2002). Beck et al. (2004) analyzed one of its pyroxenes in detail for Li abundances and isotope ratios. That pyroxene grain, mostly pigeonite, is strongly zoned in Fe* and Ti, but has nearly constant Li abundances from core to rim (Fig. 5). As with

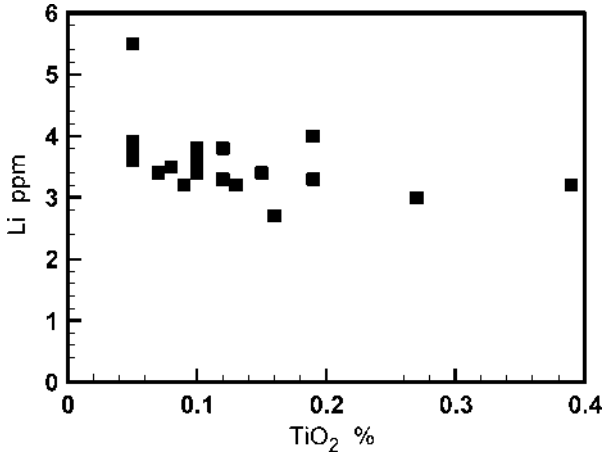

Fig. 5. Li and TiO_2 in a pigeonite pyroxene of NWA480 (data from Beck et al., 2004). Abundances of Li are effectively constant across a 10-fold increase in TiO_2.

pyroxenes in NWA 817, Nakhla, and Lafayette, the constant Li abundances in NWA480 pyroxene are not consistent with simple mineral/basalt fractionations (Table 1).

Beck et al. (2004) suggested that this constancy of Li represents a balance between Li enrichment by fractionation and Li loss to an exsolving aqueous fluid. To evaluate this hypothesis, we model evolution of the NWA480 magma as perfect fractional crystallization of pyroxene with perfect fractional exsolution of aqueous fluid. Instantaneous aliquots of crystallizing pyroxene and exsolving aqueous fluid are in equilibrium with the basalt magma, and are removed from it. First, we calculate what the bulk partition coefficient, $^{Li}D_{bulk/bas}$, must be to produce the observed Li zoning pattern in the augite. Then, we calculate the $^{Li}D_{aq/bas}$ needed to yield that $^{Li}D_{bulk/bas}$.

To calculate the $^{Li}D_{bulk/bas}$ required by this model, we apply the Rayleigh fractionation Eq. (1); if a partition coefficient D is independent of melt composition (and other changes during fractionation), then abundances of a trace element '*El*' in magma and crystals change with F, the fraction of magma remaining, according to

$$El_{melt}/El^{0}_{melt} = El_{xtal}/El^{0}_{xtal} = F^{(D-1)} \quad (1)$$

where the superscript '0' denotes the original or core composition (e.g., Richardson and McSween, 1989). To calculate F from this equation, we calculate El_{xtal}/El^{0}_{xtal} for an element that is insoluble in aqueous fluid, e.g., Ti (i.e., its bulk D is close to its mineral D). In NWA480, the TiO_2 content of its pyroxenes increases 8-fold from core to rim (Fig. 5; Barrat et al., 2002; Beck et al., 2004). Using $^{Ti}D_{pig/bas} \sim 0.15$ (Table 1) gives $F = 0.087$ for the rim, i.e., 91.3% crystallization.

The bulk partition coefficient D for simultaneous fractionation of pyroxene and aqueous fluid is given by

$$^{Li}D_{bulk/bas} = (^{Li}D_{px/bas} \cdot X_{px}) + (^{Li}D_{aq/bas} \cdot X_{aq}) \quad (2)$$

where the X are mass fraction of pyroxene and augite in the crystallizing/exsolving assemblage, and $^{Li}D_{aq/bas}$ and $^{Li}D_{px/bas} = {}^{Li}D_{pig/bas}$ are from Table 1. To derive the mass fractions (X), we assume that the parent magma was saturat-

ed with 2% H_2O when pyroxene began crystallizing and remained saturated at that level throughout fractionation (Dann et al., 2001; Lentz et al., 2001; Beck et al., 2004). We also model the process as isobaric, to avoid the pressure-dependence of water-saturation in basaltic magma. In this case, crystallization of an aliquot of pyroxene supersaturates the remaining magma in water. This supersaturation is relieved by exsolution of aqueous fluid to bring the remaining melt back to water-saturation. To maintain saturation at 2% H_2O, each gram of pyroxene that crystallizes from the magma must be accompanied by 0.0202 g of water that exsolves from the magma. Thus, $X_{px} = 0.980$, and $X_{aq} = 0.020$.

Now, one can calculate the value of ${}^{Li}D_{aq/bas}$ required to produce ${}^{Li}D_{bulk/bas} = 1$, i.e., pigeonite with constant Li abundances. Taking ${}^{Ti}D_{pig/bas} = 0.15$, and X_{px} and X_{aq} calculated above, Eq. (2) requires ${}^{Li}D_{aq/bas} \sim 45$, which is 15 times the experimentally constrained value (Table 1)! This difference in inferred and measured D values is so large as to suggest that loss of 2% water is unrealistic.

Of course, the water content of NWA480's parent magma is only estimated at 2% H_2O, based on results for other shergottites (Lentz et al., 2001; Dann et al., 2001). It is useful then to repeat this calculation for other possible water contents, even to and above the 5% level of some arc basalts on Earth (e.g., Roggensack et al., 1997; Barclay and Carmichael, 2004). The calculated ${}^{Li}D_{aq/bas}$ are given in Table 3 for this range of water contents, and are all far larger than the measured values of Table 1.

Thus, the constancy of Li in NWA480 pyroxenes cannot be ascribed readily to exsolution and loss of an aqueous fluid. As with Li in the NWA 817 augite, it is more reasonable to invoke diffusion equilibration of Li across the NWA480 pigeonites. A complicating factor for NWA480 pyroxenes, not addressed here, is their variations in Li isotopic composition. In the sole analyzed pyroxene, δ^7Li is constant at $+10‰$ except for a small core region of $-17‰$ (Beck et al., 2004). This is difficult to explain via igneous processing, but is consistent with different diffusivities for the Li isotopes (Beck et al., 2005).

5.2. Shergotty (and Zagami)

The water-loss hypothesis of McSween et al. (2001) and Lentz et al. (2001) arose from analyses of LLE in pyroxenes of the Martian meteorites Shergotty and Zagami. They found that abundances Li and B decreased from pyroxene cores to rims (their Figs. 3 and 5), and invoked exsolution and loss of an aqueous fluid to explain the decreases. The core-to-rim decreases in Li in pyroxene were confirmed by subsequent later analyses (Lentz et al., 2004; Herd et al., 2005). On the other hand, re-analyses show essentially no zoning of B abundances across the pyroxenes (Lentz et al., 2004; Herd et al., 2005).

To evaluate whether Li and B zoning in Shergotty and Zagami pyroxenes could arise during loss of an aqueous fluid, we model the crystallization of Shergotty as above for NWA480: simultaneous fractional crystallization of pyroxene and fractional exsolution of aqueous fluid. We calculate the ${}^{B}D_{aq/bas}$ and ${}^{Li}D_{aq/bas}$ required to produce the core-to-rim changes in Li and B abundances, and then compare these calculated values to experimentally determined or estimated values (Table 1).

For consistency and simplicity, we focus on the Herd et al. (2005) analyses of Shergotty pyroxenes, which include data on Ti, Li, and B (Fig. 6). In those pyroxenes, TiO_2 increases 5-fold from core to rim (Fig. 6). Because Shergotty's pigeonite and augite share the same ranges of Fe*, it is inferred that they crystallized together (Stolper and McSween, 1979; Hale et al., 1999). Shergotty contains nearly twice as much pigeonite as augite, so we calculate a combined ${}^{Ti}D_{px/bas} = 0.24$ as two-thirds ${}^{Ti}D_{pig/bas}$ and one-third ${}^{Ti}D_{aug/bas}$ (Table 1; Stolper and McSween, 1979; Hale et al., 1999). This range in TiO_2 corresponds to $F = 0.12$, or crystallization of ~88% of the magma (Eq. (1)). Over that range of fractionation, B abundances remain broadly constant in both pyroxene species (Figs. 6a and b), Li abundances in pigeonite decrease by ~2/3; and Li abundances in augite decrease by ~3/4 (Figs. 6c and d).

5.3. Boron

Boron abundances in Shergotty pyroxenes are broadly constant from core to rim (Figs. 6a and b), so their interpretation is qualitatively similar to that of Li in NWA480. We calculate ${}^{B}D_{px/bas} = 0.022$ as above for ${}^{Ti}D_{px/bas}$ (1/3 augite + 2/3 pigeonite). Assuming that all partition coefficients are constant (independent of composition and fractionation) the constancy of B abundances requires that ${}^{B}D_{bulk/bas} = 1$. To satisfy the constraints of Eqs. (1) and (2), the model for the nominal 2% H_2O requires that ${}^{B}D_{aq/bas} \approx 50$, 25 times the largest value estimated from laboratory experiments (${}^{B}D_{aq/bas} \sim 0.4$–$2.0$; Table 1). Even for 10% H_2O, the calculated ${}^{B}D_{aq/bas}$ far exceeds the laboratory values. Clearly, boron distributions in pyroxenes of Shergotty (and similarly of Zagami) are not consistent with exsolution of an aqueous fluid phase.

5.4. Lithium

For Shergotty pigeonites, the core-to-rim decrease in Li abundances fits a simple Rayleigh fractionation model (Eq. (1)). Again taking ${}^{Ti}D_{px/bas} = 0.24$, the Li/Ti curve of Fig. 6c can be modeled with ${}^{Li}D_{bulk/bas} \approx 1.6$ (see Herd et al., 2005 for a similar calculation). To calculate the required ${}^{Li}D_{aq/bas}$, we estimate ${}^{Li}D_{px/bas} = 0.22$ for crystallization of 1/3 augite and 2/3 pigeonite (Table 1). Using these values in Eq. (2) for the nominal 2% H_2O, the model would work only with ${}^{Li}D_{aq/bas} \approx 70$! This is nearly 30 times the experimentally constrained value of ${}^{Li}D_{aq/bas}$. Even for 10% H_2O, the calculated ${}^{Li}D_{aq/bas}$ far exceeds the laboratory values, suggesting that a simple water-loss hypothesis is not adequate.

Simple igneous fractionation is even less adequate in explaining Li in Shergotty augites (Herd et al., 2005).

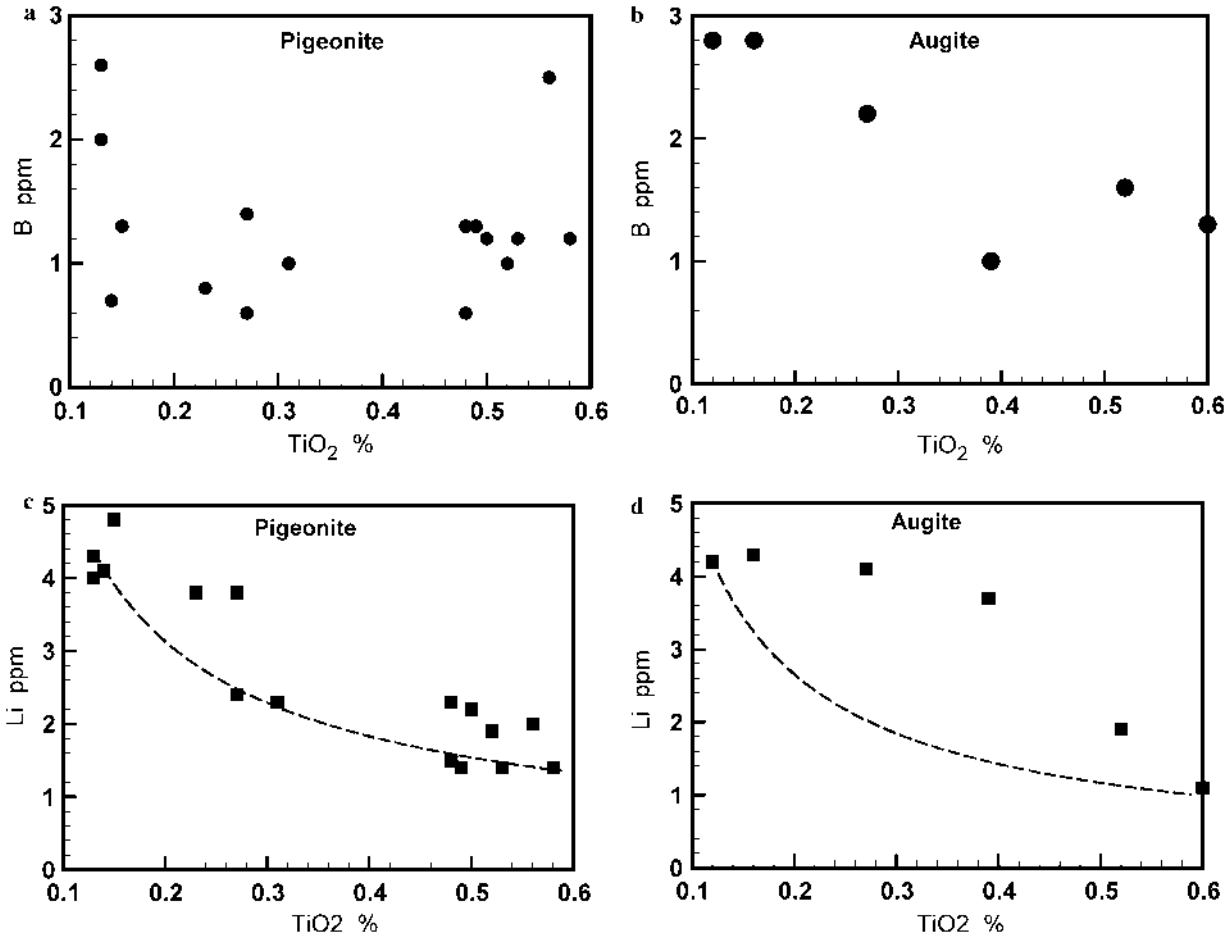

Fig. 6. Li and B zoning in pyroxenes of the Shergotty meteorite (data from Herd et al., 2005). Abundances of Ti increase 3-fold from core to rim. (a) B in pigeonite is effectively constant with increasing Ti. (b) B in augite decreases with increasing Ti. (c) Li in pigeonite decreases with increasing Ti. Dashed line shows predicted trajectory for Rayleigh fractionation with $^{Li}D_{bulk/bas} = 1.6$ (see text). (d) Li in augite decreases with increasing Ti. Dashed line shows predicted trajectory for Rayleigh fractionation and $^{Li}D_{bulk/bas} = 1.6$ (see text), which is not a good match.

To match the core and rim abundances of Li and Ti in Shergotty augites (Fig. 6d), for the nominal 2% H_2O, $^{Li}D_{aq/bas}$ must be ≈75, essentially the same problematic value as for the pigeonites. Worse, the model curve has the wrong shape. The Li–Ti trend of Fig. 6d is convex upward, but the water-loss fractionation model implies concave-upward trend (Fig. 6d). This difference between augite and pigeonite seems is consistent with a strong crystal-chemical control on Li in pyroxenes (Chaklader et al., 2005; Chaklader and Shearer, 2005), even though available igneous partitioning experiments show no such effect (Herd et al., 2004). In any case, loss of an aqueous fluid does not explain the Li abundance zoning in the Shergotty augite grains.

6. Conclusions

Zoning of the LLE in Martian meteorite pyroxenes is complicated, with at least four types of patterns, core-to-rim: sharp (constantly increasing), plateau, flat, and decreasing (Table 2, Figs. 2–6). The sharp zoning pattern in NWA 817 is consistent with 'normal' Rayleigh fractionation in igneous crystallization, based on available mineral/basalt partition coefficients (Table 1), although Li isotopic data suggest that it actually is a diffusion profile (Beck et al., 2005, 2006). The plateau pattern in NWA 817 augites is chemically consistent with igneous fractionation, although it must include some spatial inhomogeneities. However, flat and decreasing patterns are not consistent with anhydrous igneous fractionation and must have another explanation.

In most augites of NWA 817, lithium abundances are effectively constant from core to rim, i.e., a flat zoning pattern (Fig. 3). As the nakhlite parent magmas contained little water, the flat pattern is not caused by water loss. The pattern can be ascribed to intracrystalline (and inter-phase) diffusion of Li, which is consistent with the rapid diffusion of Li in basaltic melt and minerals at high temperature (Lowry et al., 1981; Giletti and Shanahan, 1997; Richter et al., 2003; Chaklader et al., 2004, 2005; Beck et al., 2005; Chaklader and Shearer, 2005). In augites of the MIL03346 nakhlite, Li abundances are zoned but Li isotopic variations show that the zoning is from diffusion and not igneous fractionation (Beck et al., 2005, 2006).

Table 2
Element zoning patterns for LLE and other elements

	Li	Be	B	Fe*	Ti
Nakhlites					
MIL03346	S	—	—	S	S
NWA 817	F, R	S, P	S, P	S, P	S, P
Nakhla	F	F	F	S, P	S, P
Lafayette	F	F	F	F	S, P
Shergottites					
NWA480	F	—	—	S	S
Shergotty	R	S	F	S	S
Zagami	R	S	F	S	S

Nakhlite meteorites arranged by decreasing cooling rate (Mikouchi et al., 2003; Treiman, 2005). Data sources described in text.
S—sharp. Abundances vary, core to rim, in accord with igneous mineral/basalt D values (Table 1), and increase monotonically from core to rim.
P—plateau. Abundances covary in accord with igneous mineral/basalt D values (Table 1), but do not increase monotonically from core to rim.
F—flat. Abundances are constant (or nearly so) from core to rim.
R—reverse. Abundances change core-to-rim opposite to that expected from mineral/basalt D values (Table 1). For these elements, abundances decrease monotonically core-to-rim.

Table 3
$^{El}D_{aq/bas}$ required, in the Text's model, to reproduce elemental zoning patterns in the meteorites' pigeonite

Meteorite		Water in parent magma			
		1%	2%	5%	10%
NWA480	Li	85	43	17	9
Shergotty	Li	136	70	27	14
Shergotty	B	98	49	20	10

See text for description of the model. See Table 1 for measured or estimated values of these D values.

Flat zoning patterns are also seen for all LLE in augite of Nakhla and Lafayette (Lentz et al., 2001). Titanium abundances show sharp, normal igneous zoning in both meteorites; Fe* shows normal igneous zoning in Nakhla augites, while Lafayette augites have nearly constant Fe*, i.e., a flat profile (e.g., Treiman, 2005). Considering isotopic and abundance zoning profiles, it seems likely that none of the nakhlites preserve original igneous zoning in Li (Beck et al., 2005, 2006, this work), whether they cooled rapidly or slowly (Treiman, 2005). Abundances of B and Be in NWA 817 augites appear to preserve igneous zoning patterns—stable isotope ratios would help greatly to confirm or refute this idea.

Simple igneous processes, with or without water, do not readily explain LLE zoning patterns in pyroxenes of the shergottite Martian basalts. The constancy of Li abundances across pyroxene in NWA480 is not consistent with low-water igneous processes. If water-saturated magma were invoked, the $^{Li}D_{aq/bas}$ required would many times the experimentally constrained values. The reverse zoning of Li in Shergotty and Zagami pigeonites exacerbates the problem by requiring that $^{Li}D_{aq/bas}$ be 30 times the experimentally constrained value. Finally the reverse Li zoning in augites of Shergotty and Zagami cannot be replicated in a simple fractionation model. Similarly, the constancy of B abundances across Shergotty pyroxenes requires $^{B}D_{aq/bas}$ be 25 times the experimentally constrained value.

How might these non-igneous patterns in pyroxene have arisen? Sub-solidus diffusion seems a reasonable hypothesis (e.g., Chaklader et al., 2004, 2005), and seems the only reasonable explanation for the Li isotopic variations within augite crystals (Beck et al., 2005, 2006). Where abundances of LLE are effectively constant (Nakhla, Lafayette, Li in NWA 817 and NWA480, B in Shergotty and Zagami), one can hypothesize sub-solidus equilibration with elements distributed according to mineral–mineral partition coefficients (e.g., Treiman, 1996). This idea seems reasonable for Li because it diffuses very rapidly in basaltic magmas (Lowry et al., 1981; Richter et al., 2003) and in feldspar (Giletti and Shanahan, 1997); data for Li diffusion in pyroxenes would be most welcome. For boron, diffusion is rather slower in magma (Baker, 1992), and its diffusion behavior in pyroxenes is not known. This diffusion of Li and B could have occurred in several types of geologic environments, including post-igneous cooling and thermal metamorphism. Effects of impact shock heating may be important for the shergottites (Chaklader et al., 2004, 2005), but not for the nakhlites (Sautter et al., 2002; Treiman, 2005).

The abundance patterns of Li and B in Shergotty and Zagami (Fig. 6; reverse or flat) could represent, as in NWA 817, presence of minor minerals that strongly concentrate Li and B. If the patterns represent sub-solidus diffusion and re-equilibration, then one only needs minerals for which $^{Li,B}D_{min/px} \gg 1$ (see Treiman, 1996). Merrillite is a possible sub-solidus host for Li but not for B, as $^{Li}D_{mer/px} \sim 3.5$ and $^{B}D_{mer/px} \sim 1.3$ (data in Herd et al., 2004). Alkali feldspar could also be important, as Li can substitute for Na, and B can substitute for Al (e.g., reedmergnerite, $NaBSi_3O_8$).

In conclusion, the behavior of Li and B in the shergottite and nakhlite Martian meteorites cannot be explained by equilibrium partitioning among common minerals, basaltic melt, and aqueous fluid. Distributions of Li and B in pyroxenes appear to be consistent with late igneous or sub-solidus diffusional equilibria or profiles, rather that reflecting the loss of magmatic water.

Acknowledgments

We are grateful to J. Jones for insightful discussions. SIMS data on NWA 817 were obtained with assistance from J. Haggerty of the Institute of Meteoritics, University of New Mexico. EMP data were collected at the ARES group, Johnson Space Center, with assistance from C. Schwandt. Critical reviews by J. Ryan and an anonymous referee improved the manuscript greatly. Financial support from NASA Cosmochemistry Grant NAG5-13279 and NASA Mars Fundamental Research Grant NAG5-12771. Lunar and Planetary Institute Contribution #1230.

Associate editor: Clive R. Neal

Appendix A

Analytical data for traverses across NWA 817 augites

Line	1	1	1	1	1	1	1	1	1	1	1	1	1	1	1
Point	#1	#3	#4	#5	#6	#7	#8	#9	#10	#11	#12	#13	#14	#15	#16
d (μm)	0.0	19.7	29.6	39.4	49.3	59.1	69.0	78.8	88.7	98.5	108.4	118.2	128.1	137.9	147.8
SiO_2	45.29	47.59	48.72	51.06	52.00	51.88	52.24	52.00	51.82	51.88	51.50	51.64	51.79	52.03	51.80
TiO_2	1.29	0.91	0.69	0.38	0.28	0.30	0.28	0.34	0.28	0.28	0.31	0.28	0.33	0.31	0.28
Al_2O_3	3.75	2.85	2.19	1.20	0.88	0.94	0.95	0.96	0.96	0.98	0.97	0.98	0.98	0.98	0.97
Cr_2O_3	0.00	0.00	0.01	0.12	0.42	0.47	0.45	0.44	0.49	0.52	0.50	0.57	0.50	0.48	0.50
FeO	26.04	23.41	20.46	16.16	13.63	13.28	13.40	13.49	13.67	13.75	13.64	13.63	13.66	13.67	13.92
MnO	0.61	0.56	0.56	0.46	0.49	0.41	0.36	0.41	0.44	0.45	0.45	0.43	0.37	0.47	0.38
MgO	3.25	5.51	7.90	11.40	12.95	13.15	13.00	12.94	12.84	13.00	12.98	12.87	12.79	12.93	12.76
CaO	18.40	18.52	18.58	19.09	19.56	19.66	19.61	19.64	19.50	19.66	19.54	19.78	19.59	19.54	19.56
Na_2O	0.44	0.45	0.42	0.35	0.31	0.33	0.34	0.35	0.36	0.34	0.33	0.30	0.32	0.34	0.33
K_2O	0.01	0.00	0.00	0.00	0.02	0.00	0.01	0.00	0.00	0.00	0.02	0.00	0.00	0.00	0.00
Sum	99.09	99.80	99.54	100.21	100.53	100.42	100.65	100.57	100.38	100.85	100.23	100.47	100.33	100.74	100.50
Fe*	81.8	70.5	59.2	44.3	37.1	36.2	36.6	36.9	37.4	37.2	37.1	37.3	37.5	37.2	38.0

Line	1	1	1	1	1	4	4	4	4	4	4	4	4	4	4
Point	#17	#18	#19	#20	#21	#68	#69	#70	#71	#72	#73	#74	#75	#76	#77
d (μ)	157.6	167.5	177.3	187.2	197.0	0	10.1	20.3	30.4	40.5	50.6	60.8	70.9	81.0	91.2
SiO_2	51.72	52.06	51.74	52.02	51.96	46.96	48.79	51.11	52.04	51.91	51.56	51.70	51.84	51.64	51.37
TiO_2	0.27	0.28	0.27	0.27	0.30	1.16	0.75	0.39	0.28	0.28	0.26	0.29	0.31	0.34	0.29
Al_2O_3	0.94	0.92	0.95	0.98	0.97	3.09	2.34	1.24	0.84	0.86	0.90	0.95	0.90	0.94	0.97
Cr_2O_3	0.51	0.49	0.48	0.50	0.50	0.00	0.03	0.12	0.34	0.42	0.45	0.42	0.52	0.46	0.46
FeO	13.72	13.68	13.63	13.48	13.58	23.94	20.25	16.42	13.45	13.30	13.38	13.43	13.46	13.40	13.66
MnO	0.49	0.36	0.47	0.46	0.37	0.60	0.57	0.33	0.37	0.48	0.47	0.40	0.39	0.42	0.45
MgO	12.88	13.11	12.77	12.80	12.78	4.80	8.00	11.36	13.10	13.10	13.01	12.96	12.98	12.86	12.81
CaO	19.50	19.45	19.61	19.71	19.61	18.98	18.91	18.95	19.65	19.75	19.53	19.68	19.70	19.64	19.61
Na_2O	0.35	0.35	0.35	0.36	0.33	0.50	0.46	0.35	0.31	0.31	0.33	0.34	0.37	0.33	0.34
K_2O	0.01	0.01	0.00	0.01	0.01	0.00	0.00	0.00	0.00	0.00	0.00	0.00	0.00	0.01	0.00
Sum	100.38	100.70	100.27	100.59	100.41	100.02	100.09	100.24	100.38	100.41	99.90	100.17	100.46	100.03	99.96
Fe*	37.4	36.9	37.5	37.1	37.3	73.7	58.7	44.8	36.5	36.3	36.6	36.8	36.8	36.9	37.4

Line	4	4	4	4	4	4	4	4	4	4	4	4	4	4	4
Point	#78	#79	#80	#81	#82	#83	#84	#85	#86	#87	#88	#89	#90	#91	#92
d (μ)	101.3	111.4	121.5	131.7	141.8	151.9	162.1	172.2	182.3	192.5	202.6	212.7	222.8	233.0	243.1
SiO_2	51.96	51.70	51.64	51.90	51.83	51.65	51.79	51.75	51.96	52.10	51.64	51.74	51.70	52.24	51.77
TiO_2	0.28	0.30	0.26	0.30	0.27	0.29	0.26	0.30	0.26	0.28	0.25	0.29	0.27	0.30	0.31
Al_2O_3	0.93	1.03	0.93	0.98	0.95	0.97	0.96	0.95	0.95	0.97	0.94	1.01	0.97	1.18	0.96
Cr_2O_3	0.51	0.47	0.49	0.46	0.43	0.41	0.44	0.42	0.44	0.41	0.46	0.49	0.43	0.45	0.50
FeO	13.51	13.56	13.45	13.57	13.68	13.65	13.57	13.70	13.55	13.52	13.66	13.55	13.43	13.30	13.74
MnO	0.39	0.45	0.45	0.38	0.44	0.40	0.42	0.49	0.35	0.48	0.41	0.46	0.48	0.34	0.55
MgO	12.90	12.95	12.83	12.94	12.81	12.93	12.90	12.81	12.92	12.06	13.07	12.91	12.91	12.53	12.95
CaO	19.62	19.50	19.70	19.61	19.35	19.42	19.46	19.47	19.58	19.61	19.48	19.42	19.48	19.15	19.50
Na_2O	0.34	0.32	0.34	0.33	0.33	0.33	0.32	0.35	0.33	0.36	0.37	0.33	0.34	0.36	0.32
K_2O	0.03	0.00	0.00	0.01	0.00	0.00	0.02	0.02	0.00	0.00	0.00	0.00	0.00	0.01	0.00
Sum	100.47	100.26	100.10	100.48	100.10	100.06	100.14	100.26	100.33	99.79	100.27	100.20	100.01	99.85	100.60
Fe*	37.0	37.0	37.0	37.0	37.5	37.2	37.1	37.5	37.0	38.6	37.0	37.1	36.8	37.3	37.3

Appendix A (*continued*)

Line	4	4	4	4	4	4	4	5	5	5	5	5	5	5	5
Point	#93	#94	#95	#96	#97	#98	#99	#100	#101	#102	#103	#104	#105	#106	#107
d (μ)	253.2	263.4	273.5	283.6	293.7	303.9	314.0	0	10.3	20.5	30.8	41.0	51.3	61.5	71.8
SiO_2	51.91	51.82	51.70	52.09	51.82	51.18	51.85	46.77	49.63	51.38	51.90	51.79	51.77	51.71	51.60
TiO_2	0.31	0.28	0.30	0.32	0.28	0.28	0.28	0.81	0.56	0.36	0.32	0.30	0.30	0.29	0.32
Al_2O_3	0.92	0.96	0.93	0.95	0.99	0.91	1.00	3.00	1.79	1.09	0.91	1.03	1.02	1.02	1.04
Cr_2O_3	0.48	0.47	0.52	0.41	0.54	0.47	0.44	0.00	0.01	0.18	0.41	0.48	0.51	0.50	0.51
FeO	13.64	13.66	13.61	13.46	13.90	13.86	13.66	25.07	19.22	15.28	13.54	13.38	13.68	13.64	13.52
MnO	0.47	0.41	0.35	0.43	0.41	0.47	0.42	0.61	0.63	0.53	0.45	0.45	0.47	0.47	0.40
MgO	12.87	13.00	12.97	12.97	13.04	12.94	13.26	4.35	9.12	12.18	12.98	12.96	13.05	13.00	12.85
CaO	19.68	19.58	19.69	19.42	19.51	18.82	19.27	18.35	19.07	19.42	19.64	19.69	19.65	19.52	19.40
Na_2O	0.32	0.35	0.31	0.34	0.35	0.35	0.33	0.47	0.42	0.37	0.30	0.33	0.34	0.35	0.35
K_2O	0.01	0.00	0.00	0.00	0.00	0.00	0.00	0.01	0.01	0.01	0.01	0.00	0.00	0.02	0.00
Sum	100.61	100.54	100.38	100.39	100.85	99.27	100.51	99.43	100.44	100.80	100.46	100.41	100.79	100.52	100.00
Fe*	37.3	37.1	37.0	36.8	37.4	37.5	36.6	76.4	54.2	41.3	36.9	36.7	37.0	37.0	37.1

Line	5	5	5	5	5	5	5	5	5	5	5	5	5	6	6
Point	#108	#109	#110	#111	#112	#113	#114	#115	#116	#117	#118	#119	#120	#121	#122
d (μ)	82.0	92.3	102.5	112.8	123.0	133.3	143.5	153.8	164.0	174.3	184.5	194.8	205.0	0.0	9.9
SiO_2	51.55	51.76	51.40	51.85	51.86	51.83	51.71	51.61	51.68	51.82	51.51	51.56	51.62	44.98	48.63
TiO_2	0.34	0.29	0.32	0.30	0.26	0.30	0.27	0.31	0.30	0.31	0.29	0.27	0.28	2.14	0.69
Al_2O_3	1.03	1.16	1.07	1.01	0.98	0.91	1.22	1.51	0.89	0.97	0.95	0.93	0.95	6.72	1.68
Cr_2O_3	0.52	0.54	0.62	0.62	0.52	0.54	0.50	0.46	0.44	0.47	0.45	0.45	0.51	0.00	0.05
FeO	13.70	14.04	13.60	13.53	13.53	13.70	13.53	13.76	13.49	13.69	13.65	13.67	13.78	24.23	22.02
MnO	0.39	0.42	0.37	0.48	0.55	0.36	0.37	0.45	0.37	0.47	0.36	0.38	0.43	0.55	0.59
MgO	12.96	12.76	12.85	13.03	13.03	13.00	12.89	12.26	12.94	13.01	12.92	13.06	12.96	1.23	6.60
CaO	19.19	19.04	19.26	19.43	19.58	19.26	19.12	18.70	19.61	19.46	19.50	19.64	19.62	18.05	18.95
Na_2O	0.32	0.35	0.36	0.35	0.36	0.39	0.33	0.35	0.33	0.32	0.31	0.33	0.36	0.95	0.39
K_2O	0.00	0.01	0.00	0.00	0.00	0.02	0.00	0.07	0.00	0.00	0.00	0.01	0.00	0.17	0.00
Sum	100.00	100.37	99.85	100.60	100.68	100.31	99.96	99.48	100.06	100.52	99.95	100.30	100.51	99.03	99.61
Fe*	37.2	38.2	37.3	36.8	36.8	37.2	37.1	38.6	36.9	37.1	37.2	37.0	37.4	91.7	65.2

Line	6	6	6	6	6	6	6	6	6	6	6	6	6	6	6
Point	#123	#124	#125	#126	#127	#128	#129	#130	#132	#133	#134	#135	#136	#137	#138
d (μ)	19.9	29.8	39.7	49.6	59.6	69.5	79.4	89.4	109.2	119.1	129.1	139.0	148.9	158.9	168.8
SiO_2	48.98	49.38	51.04	52.17	52.00	51.84	51.99	50.25	51.59	50.44	51.77	51.76	51.92	52.18	51.60
TiO_2	0.60	0.59	0.43	0.25	0.30	0.33	0.30	0.25	0.00	0.31	0.33	0.29	0.30	0.31	0.32
Al_2O_3	1.77	1.64	1.16	0.89	0.94	0.97	1.01	1.57	1.23	0.97	0.95	0.94	0.96	1.00	1.05
Cr_2O_3	0.00	0.00	0.07	0.43	0.46	0.45	0.44	0.44	0.49	0.45	0.49	0.51	0.49	0.51	0.49
FeO	21.36	20.03	16.91	13.75	13.53	13.56	13.75	13.48	13.72	13.47	13.76	13.76	13.67	13.61	13.53
MnO	0.57	0.54	0.50	0.40	0.39	0.33	0.35	0.40	0.50	0.33	0.44	0.43	0.39	0.40	0.47
MgO	7.65	8.66	11.03	13.02	13.06	13.07	13.08	14.07	12.74	12.33	12.86	12.80	12.88	12.89	12.64
CaO	18.74	18.55	19.13	19.85	19.74	19.74	19.57	19.06	19.53	19.19	19.63	19.36	19.52	19.29	19.71
Na_2O	0.37	0.40	0.36	0.31	0.35	0.35	0.34	0.31	0.35	0.33	0.33	0.30	0.35	0.35	0.34
K_2O	0.00	0.02	0.00	0.00	0.01	0.00	0.01	0.00	0.00	0.00	0.01	0.00	0.01	0.00	0.00
Sum	100.04	99.82	100.63	101.07	100.76	100.66	100.84	99.83	100.15	97.81	100.57	100.16	100.51	100.55	100.14
Fe*	61.0	56.5	46.2	37.2	36.8	36.8	37.1	35.0	37.7	38.0	37.5	37.6	37.3	37.2	37.5

(*continued on next page*)

Appendix A (*continued*)

Line	6	6	6	6	6	6	6	6	6	6	6	10	10	10	10
Point	#139	#140	#141	#142	#143	#144	#145	#146	#147	#148	#149	#227	#228	#229	#230
d (μ)	178.7	188.6	198.6	208.5	218.4	228.4	238.3	248.2	258.1	268.1	278.0	0.0	10.4	20.7	31.1
SiO_2	50.79	51.42	51.68	51.70	51.47	51.66	51.77	51.91	51.83	51.79	51.52	42.77	50.16	50.67	51.47
TiO_2	0.31	0.31	0.29	0.32	0.33	0.29	0.30	0.26	0.27	0.28	0.25	2.77	0.45	0.29	0.28
Al_2O_3	2.67	0.96	0.96	0.94	0.98	0.95	0.96	0.93	0.87	0.85	0.97	5.93	1.51	1.09	1.07
Cr_2O_3	0.47	0.47	0.49	0.48	0.48	0.47	0.48	0.46	0.42	0.41	0.27	0.03	0.03	0.47	0.51
FeO	13.15	13.46	13.81	13.76	13.73	13.76	13.50	13.43	13.34	13.48	13.99	25.60	17.73	14.50	13.51
MnO	0.40	0.45	0.41	0.45	0.38	0.44	0.40	0.50	0.47	0.48	0.47	0.57	0.44	0.39	0.38
MgO	13.19	12.71	12.95	12.99	12.85	12.91	12.93	13.04	13.16	13.10	12.82	1.52	10.51	12.75	12.87
CaO	18.89	19.65	19.55	19.36	19.47	19.47	19.70	19.63	19.64	19.76	19.53	18.98	18.67	18.40	19.19
Na_2O	0.36	0.32	0.35	0.34	0.37	0.36	0.31	0.33	0.31	0.32	0.30	0.51	0.37	0.31	0.35
K_2O	0.00	0.00	0.00	0.00	0.00	0.00	0.00	0.00	0.00	0.00	0.00	0.07	0.01	0.01	0.00
Sum	100.24	99.75	100.48	100.33	100.05	100.30	100.34	100.49	100.30	100.47	100.13	98.74	99.88	98.87	99.63
Fe*	35.9	37.3	37.4	37.3	37.5	37.4	36.9	36.6	36.2	36.6	38.0	90.4	48.6	38.9	37.1

Line	10	10	10	10	10	10	10	10	10	10	10	10
Point	#231	#234	#235	#236	#237	#238	#239	#240	#241	#242	#243	#244
d (μ)	41.4	72.5	82.8	93.2	103.5	113.9	124.2	134.6	144.9	155.3	165.6	176.0
SiO_2	51.64	51.89	51.88	52.13	51.89	50.52	50.93	51.17	50.59	50.51	49.73	47.85
TiO_2	0.33	0.32	0.34	0.29	0.31	0.28	0.26	0.37	4.43	0.48	0.57	0.76
Al_2O_3	0.96	0.95	0.93	0.95	0.95	2.24	1.13	1.03	1.25	1.41	1.53	2.57
Cr_2O_3	0.47	0.47	0.45	0.48	0.44	0.25	0.23	0.10	0.02	0.03	0.02	0.05
FeO	14.02	13.87	13.82	13.80	13.70	14.00	14.19	15.88	17.80	19.06	19.71	22.37
MnO	0.36	0.46	0.44	0.34	0.37	0.50	0.37	0.47	0.49	0.52	0.57	0.59
MgO	12.89	12.81	12.81	12.82	12.56	12.23	12.21	11.66	10.36	9.48	9.15	6.55
CaO	19.42	19.43	19.44	19.63	19.42	19.05	18.21	19.02	18.89	18.65	18.49	18.27
Na_2O	0.33	0.36	0.35	0.37	0.39	0.30	0.33	0.32	0.37	0.40	0.36	0.42
K_2O	0.00	0.02	0.00	0.00	0.00	0.01	0.03	0.01	0.00	0.00	0.00	0.03
Sum	100.43	100.57	100.44	100.81	100.02	99.38	97.89	100.03	100.21	100.53	100.13	99.45
Fe*	37.9	37.8	37.7	37.7	38.0	39.1	39.5	43.3	49.1	53.0	54.7	65.7

Line	1	1	1	1	1	1	4	4	5	5	5	5
d (μ)	0	2.5	62.5	87.5	117.5	175	7	45	17.5	37.5	55	92.5
Li	4.6 ± 0.3	6.6 ± 0.3	6.8 ± 0.5	6.6 ± 0.4	6.5 ± 0.3	6.0 ± 0.2	5.1 ± 0.3	5.9 ± 0.5	5.6 ± 0.2	5.6 ± 0.5	6.1 ± 0.4	5.8 ± 0.3
Be	0.74 ± 0.09	0.16 ± 0.03	0.03 ± 0.01	0.05 ± 0.02	0.02 ± 0.01	0.02 ± 0.01	0.41 ± 0.05	0.03 ± 0.01	0.30 ± 0.03	0.02 ± 0.01	0.02 ± 0.01	0.02 ± 0.01
B	7.8 ± 1.1	2.2 ± 0.7	0.7 ± 0.3	1.0 ± 0.3	0.5 ± 0.2	0.6 ± 0.2	3.8 ± 0.6	1.7 ± 0.6	3.5 ± 0.4	1.1 ± 0.3	1.3 ± 0.2	1.4 ± 0.2

Line	5	5	5	6	6	6	10	10	10	10	10	10
d (μ)	115	137.5	175	10	15	40	5	25	45	105	165	175
Li	5.4 ± 0.2	5.1 ± 0.2	5.6 ± 0.5	4.6 ± 0.5	4.2 ± 0.4	4.1 ± 0.4	2.2 ± 0.4	5.1 ± 0.4	5.0 ± 0.6	4.9 ± 0.3	5.1 ± 0.3	6.9 ± 0.6
Be	0.02 ± 0.01	0.02 ± 0.01	0.02 ± 0.01	0.20 ± 0.08	0.02 ± 0.01	0.06 ± 0.05	1.5 ± 0.1	0.32 ± 0.08	0.08 ± 0.03	0.04 ± 0.02	0.06 ± 0.04	0.19 ± 0.06
B	0.8 ± 0.3	0.5 ± 0.2	–	2.75 ± 0.2	1.1 ± 0.4	0.9 ± 0.3	12.9 ± 1.2	4.6 ± 0.8	0.6 ± 0.3	0.7 ± 0.2	1.1 ± 0.3	4.0 ± 1.2

Major and minor elements by EMP, LLE by SIMS; methods described in text. "Line #" refers to analytical traverses of Figs. 2 and 3. Point # for reference. '*d*' are distances in micrometers along the analytical traverses shown in Figs. 1 and 2. For LLE, uncertainties are 1σ of counting and standardization.

References

Ayers, J.C., Watson, E.B., 1993. Rutile solubility and mobility in supercritical aqueous fluids. *Contrib. Mineral. Petrol.* **114**, 321–330.

Baker, D.R., 1992. Tracer diffusion of network formers and multicomponent diffusion in dacitic and rhyolitic melts. *Geochim. Cosmochim. Acta* **56**, 617–631.

Barclay, J., Carmichael, I.S.E., 2004. A hornblende basalt from western Mexico: water-saturated phase relations constrain a pressure–temperature window of eruptibility. *J. Petrol.* **45**, 485–506.

Barrat, J.-A., Gillet, Ph., Sautter, V., Jambon, A., Javoy, M., Göpel, C., Lesourd, M., Keller, F., Petit, E., 2002. Petrology and chemistry of the basaltic shergottite North West Africa 480. *Meteorit. Planet. Sci.* **37**, 487–499.

Beck, P., Barrat, J.-A., Chaussidon, M., Gillet, Ph., Bohn, M., 2004. Li isotopic variations in single pyroxenes from the Northwest Africa 480 shergottite (NWA 480): a record of degassing of Martian magmas? *Geochim. Cosmochim. Acta* **68**, 2925–2933.

Beck, P., Chaussidon, M., Barrat, J.-A., Gillet, Ph., Bohn, M., 2005. An ion-microprobe study of lithium isotopes behavior in nakhlites. *Meteorit. Planet. Sci.* **40**. Abstract #5118.

Beck, P., Chaussidon, M., Barrat, J.-A., Gillet, Ph., Bohn, M., 2006. Diffusion induced Li isotopic fractionation during the cooling of magmatic rocks: the case of pyroxene phenocrysts from nakhlite meteorites. *Geochim. Cosmochim. Acta* **70**, in press.

Bindeman, I.N., Davis, A.M., Drake, M.J., 1998. Ion microprobe study of plagioclase-basalt partition experiments at natural concentration levels of trace elements. *Geochim. Cosmochim. Acta* **62**, 1175–1193.

Boynton, W.V., Feldman, W.C., Squyres, S.W., Prettyman, T., Brückner, J., Evans, L.G., Reedy, R.C., Starr, R., Arnold, J.R., Drake, D.M., Englert, P.A.J., Metzger, A.E., Mitrofanov, I., Trombka, J.I., d'Uston, C., Wänke, H., Gasnault, O., Hamara, D.K., Janes, D.M., Marcialis, R.L., Maurice, S., Mikheeva, I., Taylor, G.J., Tokar, R., Shinohara, C., 2002. Distribution of hydrogen in the near-surface of Mars: evidence for sub-surface ice deposits. *Science* **287**, 81–85.

Brenan, J.M., Neroda, E., Lundstrom, C.C., Shaw, H.F., Ryerson, J.J., Phinney, D.L., 1998a. Behavior of boron, beryllium and lithium during melting and crystallization: constraints from mineral-melt partitioning experiments. *Geochim. Cosmochim. Acta* **62**, 2129–2141.

Brenan, J.M., Ryerson, J.J., Shaw, H.F., 1998b. The role of aqueous fluids in the slab-to-mantle transfer of boron, beryllium and lithium during subduction: experiments and models. *Geochim. Cosmochim. Acta* **62**, 3337–3347.

Carr, M.H., Head III, J.W., 2003. Oceans of Mars: an assessment of the observational evidence and possible fate. *J. Geophys. Res.* **108** (E5), 5042. doi:10.1029/2002JE001963.

Chaklader, J., Shearer, C.K., 2005. Effects of changing pyroxene composition on Li & B behavior in lunar basalts: implications for Martian magmas. *Meteorit. Planet. Sci.* **40**. Abstract #5253.

Chaklader, J., Shearer, C.K., Hörz, F., Newsom, H.E., 2004. Volatile behavior in lunar and terrestrial basalts during shock: implications for Martian magmas (abstr.). *Lunar Planet. Sci.* **XXXV** (CD-ROM), Abstract #1397.

Chaklader, J., Shearer, C.K., Hörz, F., 2005. Li, B—Behavior in lunar basalts during shock & thermal metamorphism: implications for H_2O Martian magmas (abstr.). *Lunar Planet. Sci.* **XXXVI** (CD-ROM), Abstract #1326.

Chaussidon, M., Libourel, G., 1993. Boron partitioning in the upper mantle: an experimental and ion probe study. *Geochim. Cosmochim. Acta* **57**, 5053–5062.

Dann, J.C., Holzheid, A.H., Grove, T.L., McSween Jr., H.Y., 2001. Phase equilibria of the Shergotty meteorite: constraints on pre-eruptive water contents of martian magmas and fractional crystallization under hydrous conditions. *Meteorit. Planet. Sci.* **36**, 793–806.

Day, J.M.D., Taylor, L.A., Floss, C., McSween Jr., H.Y., 2006. Petrology and chemistry of MIL 03346 and its significance in understanding the petrogenesis of nakhlites on Mars. *Meteorit. Planet. Sci.* **41**, 581–606.

Dyar, M.D, Treiman, A.H., Pieters, C.M., Hiroi, T., Lane, M.D., O'Connor, V., 2005. MIL03346, the most oxidized Martian meteorite: a first look at spectroscopy, petrography, and mineral chemistry. *J. Geophys. Res.* **110**, E09005. doi:10.1029/2005JE002426.

Friedman-Lentz, R.C., Taylor, G.J., Treiman, A.H., 1999. Formation of a martian pyroxenite: a comparative study of the nakhlite meteorites and Theo's flow. *Meteorit. Planet. Sci.* **34**, 919–932.

Gaetani, G.A., Kent, A.J.R., Grove, T.L., Hutcheon, I.D., Stolper, E.M., 2003. Mineral/melt partitioning of trace elements during hydrous peridotite partial melting. *Contrib. Mineral. Petrol.* **145**, 391–405.

Giletti, B.J., Shanahan, T.M., 1997. Alkali diffusion in plagioclase feldspar. *Chem. Geol.* **139**, 3–20.

Gillet, Ph., Barrat, J.A., Deloule, E., Wadhaw, M., Jambon, A., Sautter, V., Devouard, B., Neuville, D., Benzerara, K., Lesourd, M., 2002. Aqueous alteration in the Northwest Africa 817 (NWA 817) Martian meteorite. *Earth Planet. Sci. Lett.* **203**, 431–444.

Greeley, R., 1987. Release of juvenile water on Mars: estimated amounts and timing associated with volcanism. *Science* **236**, 1653–1654.

Hale, V.P., McSween Jr., H.Y., McKay, G.A., 1999. Re-evaluation of intercumulus liquid composition and oxidation state for the Shergotty meteorite. *Geochim. Cosmochim. Acta* **63**, 1459–1470.

Harvey, R.P., McSween Jr., H.Y., 1992. The petrogenesis of the nakhlites: evidence from cumulate mineral zoning. *Geochim. Cosmochim. Acta* **56**, 1655–1663.

Harvey, R.P., Wadhwa, M., McSween Jr., H.Y., Crozaz, G., 1993. Petrography, mineral chemistry, and petrogenesis of Antarctic shergottite LEW88516. *Geochim. Cosmochim. Acta* **57**, 4769–4783.

Herd, C.D.K., Treiman, A.H., McKay, G.A., Shearer, C.K., 2004. The behavior of Li and B during planetary basalt crystallization. *Am. Mineral.* **89**, 832–840.

Herd, C.D.K., Treiman, A.H., McKay, G.A., Shearer, C.K., 2005. Light lithophile elements in martian basalts: evaluating the evidence for magmatic water degassing. *Geochim. Cosmochim. Acta* **69**, 2431–2440.

Hervig, R.L., Moore, G.M., Williams, L.B., Peacock, S.M., Holloway, J.R., Roggensack, K., 2002. Isotopic and elemental partitioning of boron between hydrous fluid and silicate melt. *Am. Mineral.* **87**, 769–774.

Imae, N., Ikeda, Y., Shinoda, K., Kojima, K., Iwata, N., 2003. Yamato nakhlites: petrography and mineralogy. *Antarct. Meteorit. Res. (NIPR)* **16**, 13–33.

Johnson, K.T.M., 1998. Experimental determination of partition coefficients for rare earth and high-field-strength elements between clinopyroxene, garnet, and basaltic melt at high pressures. *Contrib. Mineral. Petrol.* **133**, 60–68.

Johnston, A.D., Schwab, B.E., 2004. Constraints on clinopyroxene-melt partitioning of REE, Rb, Sr, Ti, Cr, Zr, and Nb during mantle melting: first insights from direct peridotite melting experiments at 1.0 Gpa. *Geochim. Cosmochim. Acta* **68**, 4949–4962.

Jones, J.H., Walker, D., Pickett, D.A., Murrell, M.T., Beattie, P., 1995. Experimental investigations of the partitioning of Nb, Mo, Ba, Ce, Pb, Ra, Th, Pa, and U between immiscible carbonate and silicate liquids. *Geochim. Cosmochim. Acta* **59**, 1307–1320.

Jones, J.H., 2004. The edge of wetness: the case for dry magmatism on Mars. *Lunar Planet. Sci.* **XXXV** (CD-ROM), Abstract #1798.

Karlsson, H.R., Clayton, R.N., Gibson Jr., E.K., Mayeda, T.K., 1992. Water in SNC meteorites: evidence for a Martian hydrosphere. *Science* **255**, 1409–1411.

Lentz, R.C.F., McSween Jr., H.Y., Ryan, J., Riciputi, L.R., 2001. Water in martian magmas: clues from light lithophile elements in shergottite and nakhlite pyroxenes. *Geochim. Cosmochim. Acta* **56**, 4551–4565.

Lentz, R.C.F., McSween Jr., H.Y., Fayek, M., 2004. Light lithophile abundances and isotopic ratios in shergottites (abstr.)*Lunar Planet. Sci*, XXXV. Lunar and Planetary Institute, Houston (CD-ROM), Abstract #1633.

Leshin, L.A., Epstein, S., Stolper, E.M., 1996. Hydrogen isotope geochemistry of SNC meteorites. *Geochim. Cosmochim. Acta* **60**, 2635–2650.

Lowry, R.K., Reed, S.J.B., Nolan, J., Henderson, P., Long, V.J.P., 1981. Lithium tracer-diffusion in an alkali-basalt melt—an ion-microprobe determination. *Earth Planet. Sci. Lett.* **53**, 36–40.

McDade, P., Blundy, J.D., Wood, B.J., 2003. Trace element partitioning between mantle wedge peridotite and hydrous MgO-rich melt. *Am. Mineral.* **88**, 1825–1831.

McKay, G., Schwandt, C., 2005. Mineralogy and petrology of new Antarctic nakhlite MIL 03346*Lunar Planet. Sci*, XXXVI. Lunar and Planetary Institute, Houston (CD-ROM), Abstract #2351.

McSween Jr., H.Y., Harvey, R.P., 1993. Outgassed water on Mars: constraints from melt inclusions in SNC meteorites. *Science* **259**, 1890–1892.

McSween Jr., H.Y., Grove, T.L., Lentz, R.C.F., Dann, J.C., Holzheid, A.H., Riciputi, L.R., Ryan, J.G., 2001. Geochemical evidence for magmatic water within Mars from pyroxenes in the Shergotty meteorite. *Nature* **409**, 487–490.

Mikouchi, T., Koizumi, E., Monkawa, A., Ueda, Y., Miyamoto, M., 2003. Mineralogy and petrology of Yamato 000593: comparison with other Martian nakhlite meteorites. *Antarct. Meteorit. Res. (NIPR)* **16**, 34–57.

Musselwhite, D.S., Treiman, A.H., Shearer, C.K., 2005. Light lithophile element trends in nahklite NWA 817 pyroxenes*Lunar Planet. Sci*, XXXVI. Lunar and Planetary Institute, Houston (CD-ROM), Abstract #1230.

Newsom, H.E., Shearer, C.K., Treiman, A.H., 2001. Mobile elements determined by SIMS analysis in hydrous alteration materials in the Lafayette martian meteorite*Lunar Planet. Sci*, XXXII. Lunar and Planetary Institute, Houston (CD-ROM), Abstract #1396.

Papike, J.J., 1996. Pyroxene as a recorder of cumulate formational processes: Asteroids, Moon, Mars, Earth: reading the record with the ion microprobe. *Am. Mineral.* **81**, 525–544.

Papike, J.J., Karner, J.M., Shearer Jr., C.K., 2005. Comparative planetary mineralogy: valence state partitioning of Cr, Fe, Ti, and V among crystallographic sites in olivine, pyroxene, and spinel from planetary basalts. *Am. Mineral.* **90**, 277–290.

Richardson, S.M., McSween Jr., H.Y., 1989. *Geochemistry: Pathways and Processes*. Prentice-Hall, NJ, 488 p.

Richter, F.M., Davis, A.M., DePaolo, D.J., Watson, E.B., 2003. Isotope fractionation by chemical diffusion between molten basalt and rhyolite. *Geochim. Cosmochim. Acta* **51**, 3905–3923.

Roggensack, K., Hervig, R.L., McKnight, S.B., Williams, S.N., 1997. Explosive basaltic volcanism from Cerro Negro volcano: influence of volatiles on eruptive style. *Science* **277**, 1639–1642. doi:10.1126/science.277.5332.1639.

Ryan, J.G., 1989. The systematics of lithium, beryllium, and boron in young volcanic rocks: implications for ^{10}Be. Ph.D. Dissertation, Columbia University.

Sautter, V., Barrat, J.A., Jambon, A., Lorand, J.P., Gillet, Ph., Javoy, M., Joron, J.L., Lesourd, M., 2002. A new Martian meteorite from Morocco: the nakhlite North West Africa 817. *Earth Planet. Sci. Lett.* **195**, 223–238.

Stockstill, K.R., McSween Jr., H.Y., Bodnar, R.J., 2005. Melt inlcusions in augite of the Nakhla martian meteorite: evidence for basaltic parental melt. *Meteorit. Planet. Sci.* **40**, 377–396.

Stolper, E.M., McSween Jr., H.Y., 1979. Petrology and origin of the shergottite meteorites. *Geochim. Cosmochim. Acta* **43**, 1475–1498.

Treiman, A.H., 1990. Complex petrogenesis of the Nakhla (SNC) meteorite: evidence from petrography and mineral chemistry. In: *Proc. Lunar Planet. Sci. Conf. 20th*. Lunar and Planetary Institute, Houston, pp. 273–280.

Treiman, A.H., 1996. The perils of partition: difficulties in retrieving magma compositions from chemically equilibrated basaltic meteorites. *Geochim. Cosmochim. Acta* **60**, 147–155.

Treiman, A.H., 2005. The nakhlite Martian meteorites: augite-rich igneous rock from Mars. *Chem. Erde* **65**, 203–270.

Treiman, A.H., Barrett, R.A., Gooding, J.L., 1993. Preterrestrial aqueous alteration of the Lafayette (SNC) meteorite. *Meteoritics* **28**, 86–97.

Varela, M.E., Kurat, G., Clocchiatti, R., 2001. Glass-bearing inclusions in Nakhla (SNC meteorite) augite: heterogeneously trapped phases. *Mineral. Petrol.* **71**, 155–172.

Wadhwa, M., Crozaz, G., Barrat, J.-A., 2004. Trace element distributions in the Yamato 000593/000749, NWA 817 and NWA 998 nakhlites: implications for their petrogenesis and mantle source on Mars. *Antarct. Meteorit. Res.* **17**, 97–116.

Watson, L.L., Hutcheon, I.D., Epstein, S., Stolper, E.M., 1994. Water on Mars: clues from deuterium/hydrogen and water contents of hydrous phases in SNC meteorites. *Science* **265**, 86–88.